Chemical Engineering Journal 419 (2021) 129889

Contents lists available at ScienceDirect

Chemical Engineering Journal

journal homepage: www.elsevier.com/locate/cej

SODIS potential: A novel parameter to assess the suitability of solar water disinfection worldwide

José Moreno-SanSegundo [a], Stefanos Giannakis [b], Sofia Samoili [c,1], Giulio Farinelli [d], Kevin G. McGuigan [e], César Pulgarín [f], Javier Marugán [a,*]

[a] Department of Chemical and Environmental Technology, ESCET, Universidad Rey Juan Carlos, C/ Tulipán s/n, 28933 Móstoles, Madrid, Spain
[b] Universidad Politécnica de Madrid (UPM), E.T.S. Ingenieros de Caminos, Canales y Puertos, Departamento de Ingeniería Civil: Hidráulica, Energía y Medio Ambiente, Unidad docente Ingeniería Sanitaria, c/ Profesor Aranguren, s/n, Madrid ES-28040, Spain
[c] European Commission, Joint Research Centre (JRC), Seville 41092, Spain
[d] Department of Environment, Land and Infrastructure Engineering (DIATI), Politecnico di Torino, Corso Duca degli Abruzzi 24, 10129 Turin, Italy
[e] Department of Physiology & Medical Physics, RCSI University of Medicine and Health Sciences, Dublin 2, Ireland
[f] School of Basic Sciences (SB), Institute of Chemical Science and Engineering (ISIC), Group of Advanced Oxidation Processes (GPAO), École Polytechnique Fédérale de Lausanne (EPFL), Station 6, CH-1015 Lausanne, Switzerland

ARTICLE INFO

Keywords:
Solar Disinfection (SODIS)
Predicted time-varying incident radiation
Worldwide temperature profile
Inactivation modelling
World maps
E. coli

ABSTRACT

This paper studies the worldwide applicability of solar water disinfection (SODIS) technology through a novel parameter: the SODIS potential. This parameter is defined as the inverse ratio between the required exposure time to achieve a four log disinfection of *E. coli* and the six hours recommended by the standard SODIS protocol. The *E. coli* inactivation kinetics was predicted by fitting the results under different temperature and incident radiation to a semi-empirical inactivation model, including a synergy term between bacterial stress sources (light/heat). To estimate the SODIS potential, a solar calculator was developed based on the Sun's position, atmospheric extinction, cloud-cover, and elevation. The time-varying total incident radiation available at any location worldwide was estimated for each day along the year during sunlight hours. The time-varying temperature was also estimated from minimum and maximum values, introducing its dynamic variation along with the solar exposure of the water. Both incident radiation and temperature values are input into the kinetic model to estimate the disinfection rate. Based on these values, the number of batch disinfections that can reach the goal of 99.99% bacterial elimination in 1 day and the minimum daily time required to achieve this goal is computed; the latter is finally transformed to the SODIS potential. The results of the study, illustrated as contours indicating the SODIS potential and other relevant indicators overlayed on a world map, confirm that latitude has a significant contribution to the SODIS potential, with the highest values close to the equator. However, the results also highlight the importance of temperature and cloud-cover, with critical differences between equal latitude regions.

1. Introduction

Solar disinfection (SODIS) is a standard water treatment method used by communities where access to safe drinking water is a problem [1]. Water is exposed to sunlight radiation in a transparent container, usually a bottle or bag (typically of 1.5 or 2 L volume) for at least 6 h under sunny conditions. SODIS has been demonstrated to reduce waterborne pathogens, such as bacteria, viruses, fungi and protozoa [2]. In 2009, SODIS was in daily use by more than 4.5 million people along 55 countries in Asia, Latin America, and Africa [3].

The mechanism of action for SODIS consists of multiple processes acting simultaneously, resulting in the inactivation of the microorganisms. It is accepted that UV-B damages DNA [2], but represents only a small contribution in SODIS inactivation of microorganisms, since 95% of the UV-B range is absorbed by stratospheric ozone. Furthermore, the materials of the vessels used might further reduce UV-B transmittance [4]. Consequently, the UV-A portion of sunlight is the main inactivation

* Corresponding author.
E-mail address: javier.marugan@urjc.es (J. Marugán).
[1] Disclaimer: The views expressed are purely those of the author and may not in any circumstances be regarded as stating an official position of the European Commission.

https://doi.org/10.1016/j.cej.2021.129889
Received 17 January 2021; Received in revised form 25 March 2021; Accepted 14 April 2021
Available online 20 April 2021

Nomenclature

AM	*Air mass*, thickness of the atmospheric layer to be crossed by sunlight.
CFD	*Computational fluid dynamics.*
CRU	*Climatic Research Unit* of the University of East Anglia.
DHI	*Diffuse horizontal irradiation*, contribution of the diffuse radiation to the GHI.
DNI	*Direct normal irradiation*, direct radiation measured parallel to the beam direction.
GHI	*Global horizontal irradiation*, radiation energy reaching the Earth surface, measured as the vertical component of both direct and diffuse irradiation.
GRG	*Generalised reduced gradient.*
MTI	*Maximum theoretical irradiation*, total incident radiation under clear sky conditions, considering only the atmospheric extinction.
NREL	*National Renewable Energy Laboratory.*
NRMSLE	*Normalised root mean squared logarithmic error.*
ROS	*Reactive oxygen species.*
SODIS	*Solar water disinfection.*
SPA	*Solar positioning algorithm.*
TIR	*Total incident radiation*, photon flux crossing a point from all possible directions. This magnitude is referenced to a volume, while flux (or GHI) are referenced to a surface. The chance of a photon being absorbed by a target compound, triggering a photoactivated reaction, is proportional to this magnitude.

factor of SODIS [5]. UV-A light induces the production of reactive oxygen species (ROS) inside the cell, whose accumulation ultimately leads to cell-death [5-7]. Temperature also strongly affects the solar disinfection process, inducing a synergetic effect with sunlight that shortens the treatment time with increased temperature values, especially for values above 45 °C [8]. The direct effect of temperature can be related to the denaturation of bacterial proteins [9], while the synergetic effect can be related to faster steps in the whole mechanism of radiation damage.

Therefore, the efficacy of the process is highly dependent on available solar radiation, temperature, and variables with high geographic and seasonal variability. The irradiance incident on a horizontal surface at ground level reduces in a cosine rate as latitude increases away from the equator. Furthermore, variations in weather patterns have to be considered; for example, the cloud-cover considerably affects the radiation received. Consequently, a general recommendation is that, for cloudy conditions, bottles should be exposed for two consecutive days to solar radiation [2], rather than 6 h.

Although the efficacy of SODIS against various microorganisms has been studied in-depth for a range of different pathogens since the 80′s, to the best of our knowledge, there are no predictive methodologies available for the expected effectiveness of the process worldwide. No previous attempts have been reported to correlate the disinfection potential obtained in different locations based on the measured radiation and temperature data. One reason for this is the lack of available daily or monthly average incident radiation data, on which predictive models can be easily applied. Available data in public databases are limited to annual averages of direct, diffuse or global horizontal irradiation, focused on predicting solar capacity for application in the photovoltaic field. Cloud-cover is included in these global values, but indirectly.

Concerning the first part, the calculation of the solar vector (its relative position to an observer on the surface of the Earth) is well established. There are relatively simple models based on the solar vector to estimate the incident radiation (direct and diffuse) for a specific location and hour of the day [10,11]. The *Fair Weather Condition* model, available in some CFD tools for obtaining a prediction of the incident and diffuse radiation [12], does not include cloud-cover, but rather the possibility of specifying a value set by the user or approximating an average value. Several more complex models are reported in the literature, but they are mainly based on soft computing with a high number of parameters and terms with no physical meaning [13,14], which is often the drawback in empirical approaches of SODIS modelling. Moreover, it is important to establish the link between the solar irradiation simulation and how well laboratory disinfection data, acquired in controlled conditions, fit to expected SODIS efficacy in the field.

The present work reports the development of a tool for the simulation of the efficacy of SODIS processes, based on the description of the expected time-varying sunlight and air temperature at any specific location around the world. An improved model to estimate incident radiation is presented, which calculates the solar vector and modifies the clear sky irradiation as a function of cloud-cover and latitude. The model is designed to offer transient predictions depending on the time of the day. Yearly averaged values are validated against the open maps of direct and diffuse incident radiation available in the *Global Solar Atlas*, provided by the *World Bank Group*. Estimation of time-varying temperature is also included in the developed tool. In addition, a kinetic model for *E. coli* solar disinfection is proposed, including the dependence of the process on incident radiation and temperature, and integrated into the previously developed tool. As a case study, a full year was modelled using 90 timesteps per day around the world, using instantaneous values of radiation and temperature in the developed kinetic model, in order to predict the achieved inactivation of *E. coli*. Finally, the "SODIS potential" concept was introduced to analyse the results and give an indicative value of the suitability of the process at a given location. The main novelty and relevance of this work is not only the estimation of the SODIS potential to assess the suitability of solar water disinfection process to provide drinking water in a specific region of the world, but also the development of a general and modular methodology that can be easily customised to assess in a similar way any other solar photoactivated process and application.

2. Model development

2.1. Kinetic modelling

Briefly, a subset of a broader design of experiments studying solar inactivation of *E. coli* as a model faecal bacterial microorganism has been used, in which the inactivation was obtained under different conditions of i) solar irradiation (between 0 and 1200 W m^{-2}), and ii) temperature range in the microbial medium (between 20 °C and 50 °C). Experiments were performed in duplicates as biological replicates (separate occasions), with a standard deviation below 15%. The complete experimental procedure and a detailed analysis of the disinfection data collected from the kinetic study are available as an open dataset [15]. This wide range of experimental conditions has been then integrated into a kinetic model that can consider both the thermal effect and the photonic effect (photolytic) on *E. coli* to estimate the disinfection rate. These two variables have been previously shown to have the most significant effect on the efficacy of the disinfection process [16].

Most widely used disinfection models are empirical equations based on Chick's law [17], or Hom's model (a modification of Chick's law that considers the "shoulder" (lag phase) often present in this microbial behaviour. Hom's model is chosen, as the data present a shoulder even in the logarithmic plot, and it is described as follows [18]:

$$log_{10}\left(\frac{C}{C_0}\right) = -k_{exp}t^n \quad (1)$$

where k_{exp} is an experiment specific kinetic constant, t is time, n is a dimensionless global exponent of time for all experiments, and C/C_0 is

the relation between instantaneous and initial concentrations in the experiment. The units of the constant depend on the time units so that the global expression remains dimensionless. A seed value of n is proposed for the global set, and in every experiment $log_{10}\left(\frac{C}{C_0}\right)$ is linearly fitted to t^n. This gives a set of modelled values at every time that can be compared to the experimental ones. The value of n is then optimised using a GRG nonlinear algorithm to minimise the sum of squared differences between modelled and experimental values. It must be noted that the fitting of each experiment with its own independent value of k_{exp}, has a minimal error, much lower than the final model, whose global target is to predict this k_{exp} value from temperature and radiation.

The time exponent of the kinetic model was optimised using a generalised reduced gradient (GRG) nonlinear algorithm [19] to minimise the differences between experimental data, and a log-linear dependency on time raised to the n power. An optimum solution is reached when the partial derivatives of the objective and constraint functions reach zero. The optimisation algorithm ensures the global optimum identification, as the sequence of input values is monotonic. The remaining kinetic parameters for the proposed kinetic model for *E. coli* solar disinfection were optimised using linear regression, producing, in addition, an estimation of the standard error of each parameter. The regression of the model was minimised using the normalised root mean squared logarithmic error (NRMSLE) for the cultivable bacteria concentration, obtained experimentally and predicted by the model.

k_{exp} values were modelled as a function of radiation intensity and temperature. The values of k_{exp} must be explained from the combined effect of temperature and irradiance. Experimental results showed that inactivation occurs in dark conditions at high temperatures, indicating that a thermal term independent of radiation must also be included. To consider temperature dependence, k_{exp} values in dark conditions were fitted to the Arrhenius equation, modifying Eq. 1 to:

$$log_{10}\left(\frac{C}{C_0}\right)_{dark} = -k_{T,dark}\exp\left(\frac{-Ea_{T,dark}}{RT}\right)t^n \quad (2)$$

Where $k_{T,\ dark}$ is the Arrhenius pre-exponential factor (min^{-1}),

$Ea_{T,\ dark}$ is the activation energy of the thermoactivated reaction (J mol^{-1}),

T is the temperature (K), and

R, the universal gas constant (8.314 $J{\cdot}K^{-1}{\cdot}mol^{-1}$).

A multi-hit approach [20] (i.e. the inactivation of a cell is the result of many hits on specific target(s)) is selected to model the nonlinear dependency of the inactivation rate with radiation, introducing an exponent α to the irradiation term. The synergy has been included using an Arrhenius-like constant in the photo-activated term. The optical activation of a compound is independent of temperature, as photon energy is not dependent on it. In terms of bacterial inactivation, if the photonic activation is only the first step in the disinfection process, because photoactivated compounds need to collide with specific targets in the bacteria, the probability of interactions at a given energy will follow Arrhenius' law (Equation 3). This could be a valid assumption, given that inactivation is an intracellular, reactive oxygen species (ROS)-mediated process that is initiated with the photonic inactivation of ROS-scavenging enzymes [21].

$$log_{10}\left(\frac{C}{C_0}\right) = -\left(k_{Syn}I^{\alpha}\exp\left(\frac{-Ea_{Syn}}{RT}\right) + k_{T,dark}\exp\left(\frac{-Ea_{T,dark}}{RT}\right)\right)t^n \quad (3)$$

2.2. Radiation and temperature datasets

To complete the SODIS efficacy simulation tool and to validate the results, yearly averaged maps of radiation were downloaded from the *Global Solar Atlas* [22], provided by the *World Bank Group* [23]. Modelled solar and meteorological data are available for all land areas from 60°N to 45°S. They are provided under the Creative Commons 4.0 license, which allows users to share (copy and redistribute the material in any medium or format) and adapt (remix, transform, and build upon the material for any purpose, even commercially). The Solargis model (used for all calculations behind Global Solar Atlas) has been so far validated at 228 public sites worldwide. More than 20 different networks across the globe have been used by Solargis for the performance validation of satellite-based models.

Monthly averaged temperature and cloud coverage percentage worldwide was obtained from the open database of the Climatic Research Unit, University of East Anglia [24]. Version 4 of the CRU TS monthly high-resolution gridded multivariate climate dataset was used [24]. Data are available from 1901 to 2019. All land areas are provided (excluding Antarctica) at 0.5 ° resolution. Table S1 in the supplementary information summarises the different datasets downloaded from the Atlas and the CRU.

To validate the proposed equation to include the hourly dependence between the minimum and maximum temperature values, weather forecast data for several days and cities in one of the most commonly used applications have been consulted [25].

2.3. Modelling of time-varying temperatures

Monthly average temperature values were available in the CRU database (see section 2.2 for further details). However, the nonlinear dependency kinetics with irradiation or temperature, and the synergy effect between them, hinder the use of average values, requiring transient data. In addition, the average temperature combined day and night values, which for a sunlight-based process would lead to the underestimation of the process. Hence, the main target of this step is to obtain time-varying values of temperature at different locations in the world. Although the temperature values used in the model correspond to air temperature 1.5 m above ground, the temperature of the air closer to the ground shows minor differences with the used values [26].

General temperature trends throughout a month can be considered approximately constant from year to year, while periods of weeks or days seem to be too short to be used. Consequently, monthly average values of minimum and maximum daily temperature were used for prediction.

Daily temperature trends for different cities worldwide were studied to define a simple model that allows estimating time-varying temperature from available data, with no empirical parameters involved. Equation 4 shows the chosen model, a sine wave depending on sun transit, maximum temperature and minimum temperature.

$$T(h) = \frac{T_{max}+T_{min}}{2} + \frac{T_{max}-T_{min}}{2}\sin\left(\frac{\pi}{12}(h - h_{dawn} - 0.25(h_{sunset} - h_{sunrise}))\right) \quad (4)$$

Where: $h_{sunrise}$ and h_{sunset} are the times of sunrise and sunset in local time, obtained by the solar positioning algorithm, h is the local time, and T_{max} and T_{min} are the monthly-average of daily minimum and maximum data from the CRU database used by the function to calculate the transient value $T(h)$.

2.4. Solar vector and maximum theoretical radiation calculation

As stated before, time-varying radiation values are required for use in the kinetic model. Only yearly averages of daily totals are available in the database of *Global Solar Atlas*. However, photoactivated reactions are triggered by photon absorption, and thus their kinetics directly depends on the availability of photons crossing each point. Hence, the incident radiation is estimated from the available data.

The NREL SPA algorithm [27,28] allows us to calculate the solar vector compared to the earth surface normal for each location at any given date-time. Using the zenith angle from the solar vector, the Young 1994 equation (Eq. 5) [29] allows us to determine the relative

atmospheric depth crossed by sun rays (Air mass, AM).

$$AM = \frac{1.002432cos^2 z_t + 0.148386\cos z_t + 0.0096467}{cos^3 z_t + 0.149864cos^2 z_t + 0.0102963\cos z_t + 0.000303978} \quad (5)$$

AM is the depth of the atmospheric mantle crossed by the sun rays relative to its size when the Sun is at zenith (AM 1.0). Values can vary from 0.0 (radiation reaching the Earth's atmosphere) to 43.0 (at dawn or dusk) [30]. However, the most used values for estimations are AM 1.0 (midday during equinox at the equator, minimal atmosphere depth) and AM 1.5, which corresponds to the standard atmosphere depth, used for solar energy applications as an overall yearly average in mid-latitudes.

Spectra AM 0.0, AM 1.0 and AM 1.5 [27] were fitted to a wavelength-specific Lambert-Beer model (Eq. 6), obtaining atmospheric extinction coefficients with a precision of 1 nm in the wavelength, where $I_{0.0,\lambda}$ is the spectra obtained from the AM 0.0.

$$I_{AM,\lambda} = I_{0.0,\lambda} e^{-\kappa_\lambda AM} \quad (6)$$

The extinction coefficients (κ_λ) have units of AM^{-1}, as they are intended to be used in conjunction with the NREL spa algorithm and the Young equation to get the spectrum at a given location, date, and time. Then, the spectrum is integrated over wavelength to get the total incident radiation. The whole solar spectrum is currently used, but the developed software can be used in any wavelength interval. Afterwards, the radiation data is adjusted using solar distance (±8% throughout the year), also obtained from NREL's SPA algorithm. This method gives the maximum theoretical irradiance (MTI) values for time-varying direct solar irradiation, but does not include cloud-cover effect. A scheme with the calculation process before the integration of the cloud-cover is available in Fig. 1.

2.5. Impact of cloud-cover on radiation

The calculated maximum theoretical irradiation (MTI) predicts maximum irradiation on sunny days, attenuated by cloud-cover. The Reed [31] and Angström models [32] are the most widely used in literature to estimate direct normal radiation (DNI) from cloud-cover (C) and MTI (equations 7 and 8, respectively):

$$DNI = (a - bC - c\alpha_{noon})MTI \quad (7)$$

$$DNI = (a - bC)MTI \quad (8)$$

Where:

a, b, c are specific parameters of the models and

α_{noon}, is the daily minimum solar zenith angle in the given latitude.

Both models were fitted with the available data (DNI), obtaining a normalised root mean square error (NRMSE) of 28% and 22.7%, respectively, compared to Global Solar Atlas data.

A novel variation of the Reed model has hereby been developed that reduces the NRMSE to 20.8% in the prediction of DNI. However, the novelty of this model is that it also fits DHI using the same variables and allows its use in the calculation of global radiation variables, such as TIR or GHI. It is also a simple model of three parameters, meaning that every term has a high statistical significance. Cloud-cover factor formula for DNI and DHI are presented in Equations 9 and 10, respectively.

$$DNI = (a_{DNI} - b_{DNI}C - c_{DNI}\sin(4lat + 1.2))MTI \quad (9)$$

$$DHI = (a_{DHI} - b_{DHI}C - c_{DHI}\sin(4lat + 1.2))MTI \quad (10)$$

The first two terms are common with the Reed and Angström models, setting the linear decrease of DNI with cloud-cover. The third term describes the dependency on latitude, similar to the term appearing in the

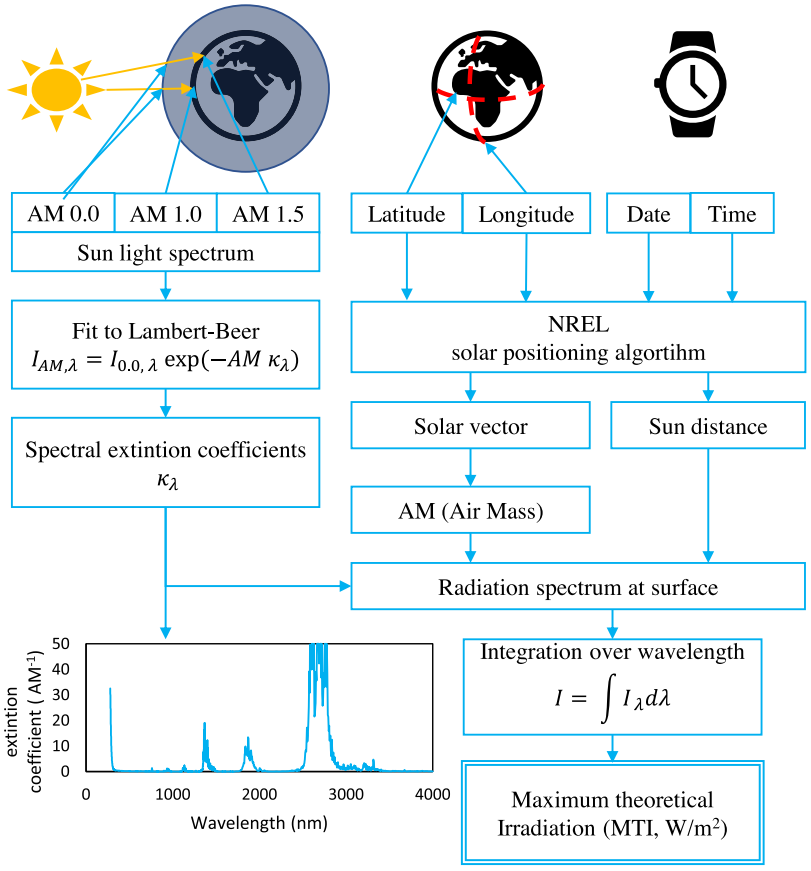

Fig. 1. Required input (top) and algorithm steps to produce time-varying radiation data (maximum theoretical irradiation).

Reed model but based on the global atmospheric streams. This term reaches maximum values at the Hadley cell (latitude below 30°) and Polar cell (latitude above 60°), with a dryer climate, and minimum values at the Ferrel cell (latitude 30-°) with moderate to high humidity. The function is slightly displaced to North, as it is the division between both Hadley cells, due to the higher heating of the northern hemisphere [33].

The data for the independent variables (MTI, C·MTI, sin(4lat + 1.2) · MTI) are produced for every location, using 90 timesteps for each day of the year. Daily values are integrated over time and averaged over a one-year period. The yearly averages of daily totals are linearly fitted to equations 9 and 10, and model parameters are obtained. The parameters can be used to obtain time-varying DNI and DHI values from corresponding MTI values and day cloud-cover. A general scheme of the integrated irradiation/cloud-cover data production is present in Fig. 2.

Finally, global radiation variables can be calculated from direct and diffuse components of solar light (Eq. 11 and 13).

$$GHI = DHI + DNI\cos z_t \tag{11}$$

Considering diffuse sunlight as isotropic, the diffuse irradiation contribution (DIC) to total incident radiation (TIR) is twice the DHI, as shown in equation 12, and TIR can be estimated by adding to this value the DNI (Eq. 13).

$$DHI = \int_0^{\pi/2}\int_0^{2\pi} \frac{DIC}{4\pi} cos\theta \, d\theta \, d\varphi = \frac{DIC}{2} \tag{12}$$

Where $\frac{DIC}{4\pi}$ is the radiation intensity of diffuse light in each direction. Its vertical component ($\frac{DIC}{4\pi}\cos\theta$) is integrated over all directions represented by spherical coordinates (φ and θ).

$$TIR = DNI + DIC = DNI + 2DHI \tag{13}$$

2.6. Computational details and software used

Data were read from GIS format files, normalised, and/or interpolated to the desired grid of 0.5° in latitude and longitude, using a developed C^{++} tool. It also averages CRU data of the last 8 years to a single "average year" to minimise the deviation of the model when required to extrapolate to any desired year.

The tool includes the solar positioning algorithm (SPA) from NREL [27,28] and developed functions to: i) estimate atmospheric extinction coefficients; ii) get transient irradiation values, both theoretical maximum at sunny days and those corrected by cloud-cover; iii) get transient temperature; iv) generate yearly averaged values, to adjust cloud impact parameters; v) estimate disinfection rate, a function which can be easily replaced to use the tool in different processes or different kinetic models; and vi) generate monthly averaged results of the disinfection. In this work, the results of the model predictions are analysed in terms of the number of batches per day reaching a 4-log inactivation in each batch (as recommended by the WHO) [34], the minimum exposure time required to achieve this inactivation level, and the SODIS potential.

The developed code is openly available at the Github and Zenodo repositories [35].

3. Results and discussion

3.1. Kinetic model fitting

Fitting dark reactions and values of $k_{T,dark}$ and $Ea_{T,\ dark}$ separated from irradiated experiments reduces the degrees of freedom of the global model fitting and increases the consistency of parameters. The linear fitting of dark experiments achieved an r^2 value of 0.94.

When comparing experiments in Fig. 3B, C, or D to dark experiments (Fig. 3A), it can be seen that the differences attributed to temperature are higher as irradiance increases, meaning that there is a synergy between both sources of stress. This kind of synergy has been previously observed between temperature and radiation [36] and between radiation and other bacterial stress sources [37]. Fig. 3(E-H) shows the same experimental data as Fig. 3(A-D), but with experiments grouped by temperature to observe the effect of radiation.

The modelled inactivation results are presented in Fig. 3 **(lines)** for comparison with the experimental data. A summary of the calculated kinetic parameters for the model obtained are presented in Table 1. The fitting of irradiated experiments with the complete model shows an r^2 value of 0.85. The model achieved estimations with an NRMLSE of 17.9%. The global error obtained was considered sufficiently acceptable even though it is based on a semi-empirical model with a limited number of parameters. Furthermore, although the inactivation experiments took place under controlled conditions of irradiance and temperature, we highlight that natural surface water was used (Lake Geneva water), spiked with a wild type *E. coli* strain and subjected to SODIS. As a result,

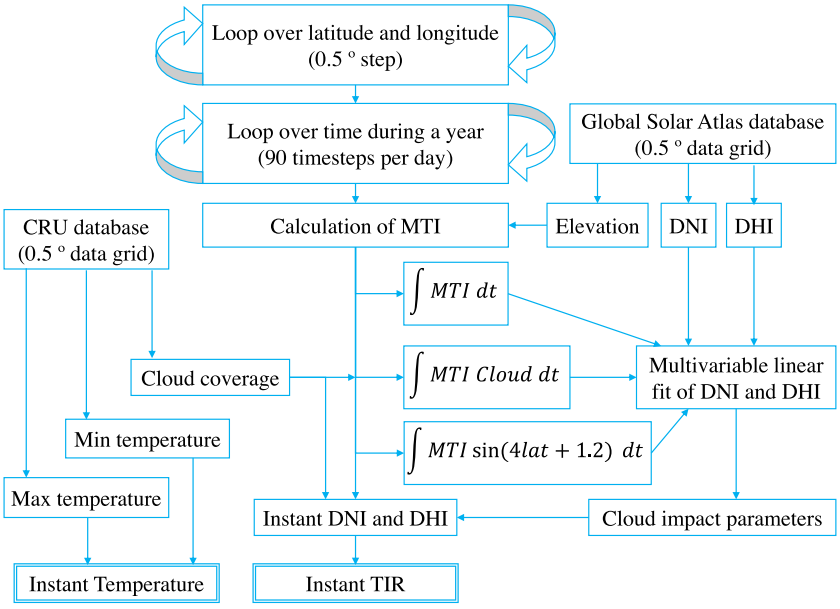

Fig. 2. General scheme of integrated irradiation/cloud-cover data production.

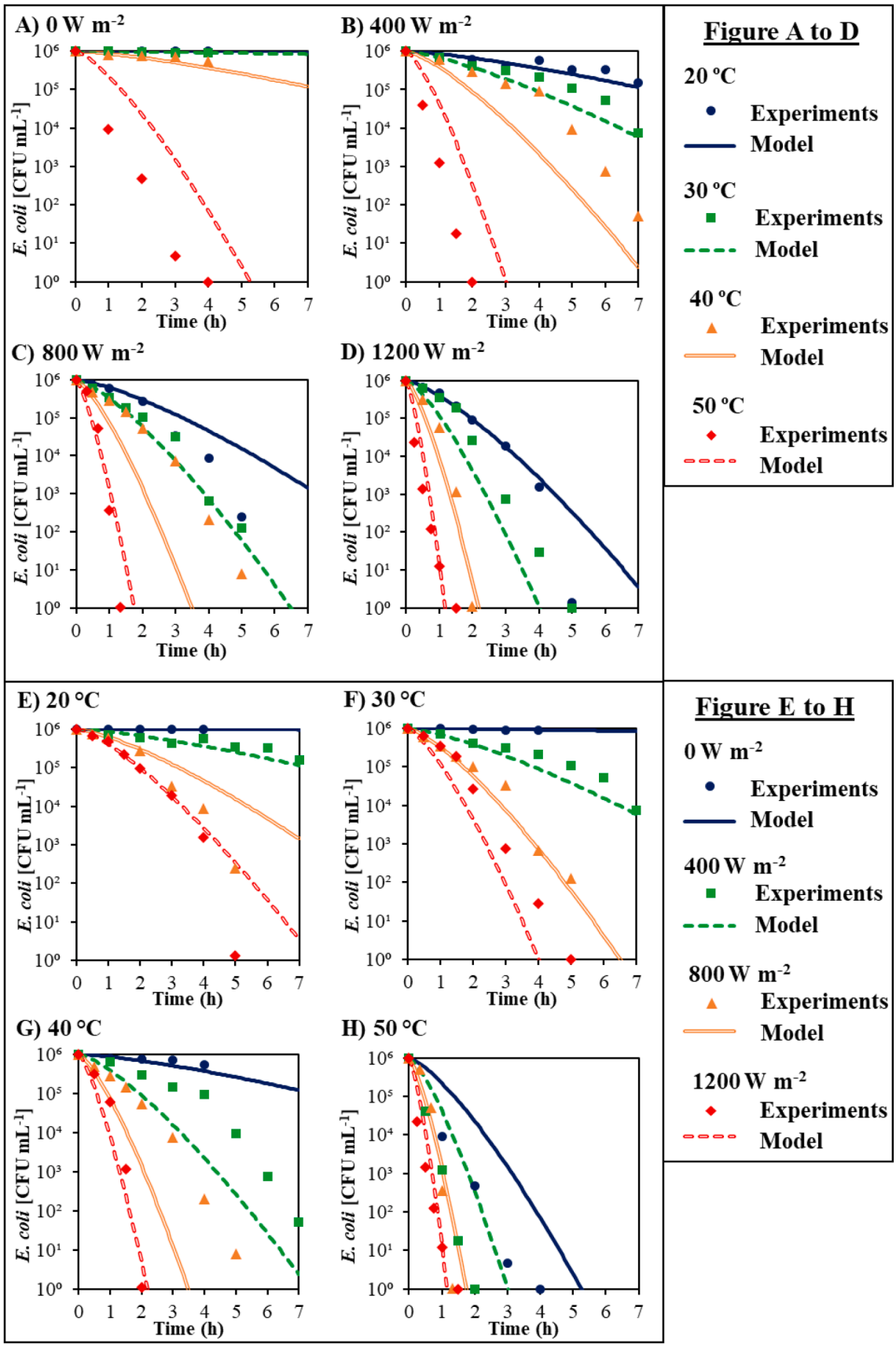

Fig. 3. Correlation between experimental data (dots) and model predictions (lines) for the bacterial inactivation with the SODIS process. Plots are grouped by radiation intensity (A-D) and temperature (E-H).

Table 1
Kinetic parameters obtained for the *E. coli* SODIS inactivation.

Kinetic parameter	Value	Units	Correlation with NMRSE
$k_{T,\ dark}$	$1.14 \times 10^{28} \pm 8.76 \times 10^{7}$	$min^{-1.3405}$	4.8%
$Ea_{T,\ dark}$	189 ± 47	$kJ\ mol^{-1}$	−71.4%
N	1.3405	–	32.5%
k_{Syn}	1800 ± 140	$m^2\ W^{-1}\ min^{-1.3405}$	0.2%
Ea_{Syn}	61.6 ± 11.2	$kJ\ mol^{-1}$	−2.7%
α	1.61 ± 0.35	–	1.9%

17.9% of NRMLSE is considered a satisfactory value, including the variability of the water source (in solids, organic matter, ions content, etc.).

The worst predicted series are those combining low irradiation and high temperatures. The shoulder observed in most experiments disappears there, and the model predicts slower disinfection than the actual experiments. Using two different time exponents for the thermal and radiation terms would improve the predictions in those situations but hinders the fitting and use of the model. However, those cases are extremely rare, as the highest temperatures are expected just after midday, together with high irradiation. Thus, the error in those series can be reasonably assumed from a practical point of view.

A rigorous mechanistic model could improve the fit and increase the extrapolation capacity of the model at the expense of a significantly higher computational time. Therefore, for the purpose of this work, which is the production of SODIS potential maps, this kinetic fitting is considered sufficient as a proof of concept. In any case, the developed procedure is available for the future coupling of any other kinetic approach, including other microorganisms such as viruses, protozoa, etc.

3.2. Validation of time-varying temperatures worldwide

Fig. 4 shows the agreement between the temperature trend and the model estimation for selected cities around the world on a specific day. The model has been further verified for different dates throughout the year, with similar results in various seasons (data not shown).

Table S2 in the Supplementary Information shows the NRMSE between modelled and forecasted temperatures and the improvement using the modelled temperature values instead of a constant average temperature. This improvement is especially relevant considering the exponential dependence of the chemical reaction rates on temperature. Specifically, the error is halved if a whole day is observed and reaches a 60% reduction when only sunny hours are studied. This improvement is observed in most of the selected cities, with some exceptions in locations such as Cartagena or Mumbai, where the temperatures remain almost constant in a narrow range of 2–3 °C. In any case, in these places the NRMSE is already below 4% with or without using the predictive model for transient temperatures, hence the improvement is factual in places where the error would be high.

The model was designed using integer or simple rational numbers instead of fitting data to a more complex model, and thus, no statistics of the model are shown beside the obtained NRMSE.

3.3. Validation of model predictions for global radiation magnitudes

From the above calculation, we can obtain the modelled Direct

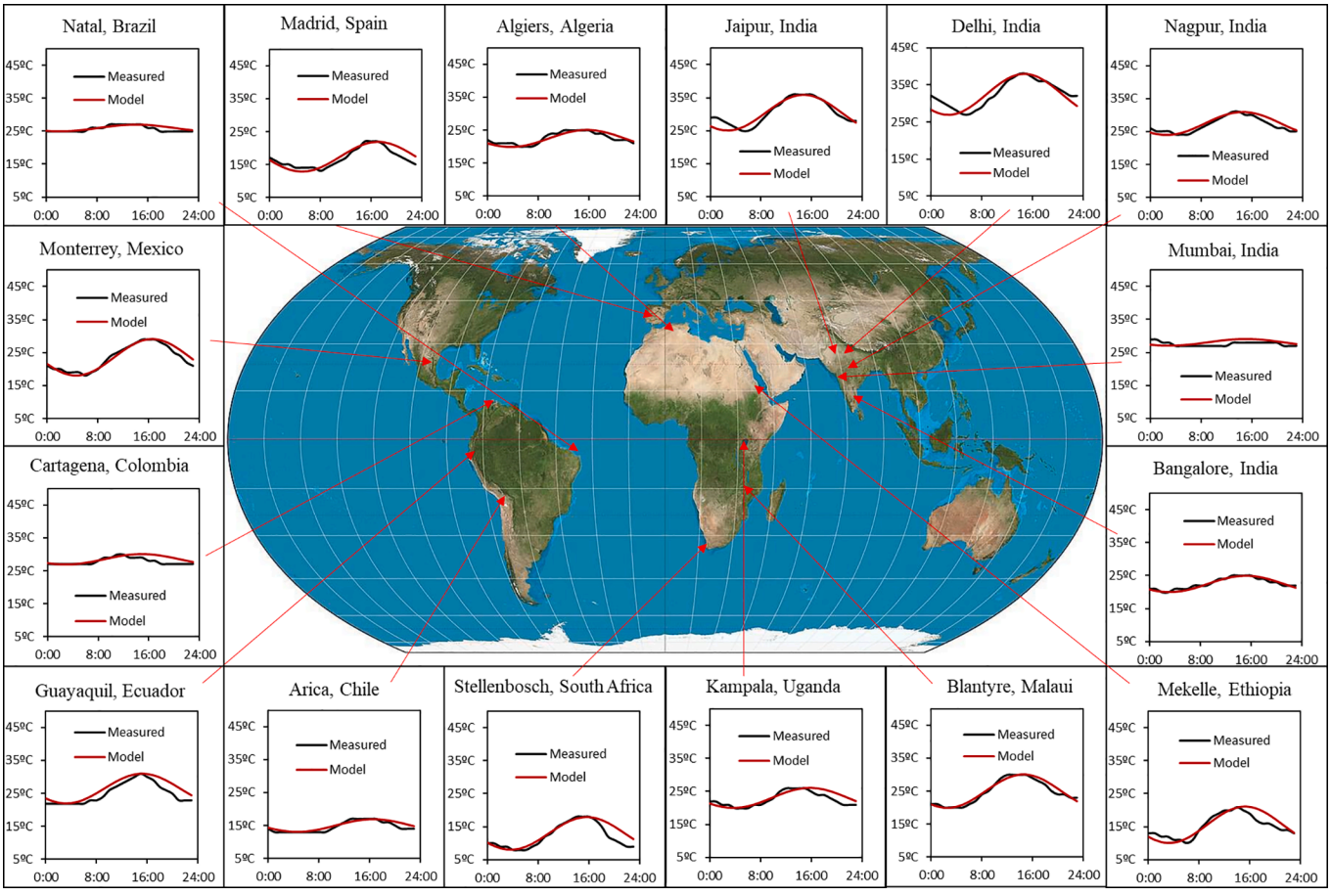

Fig. 4. Validation of the predictions of the temperature model in sixteen selected cities. Predicted temperature vs weather forecast, 21st September 2020.

Normal Irradiation (DNI) and Diffuse Horizontal Irradiation (DHI) values. Fig. 5 shows a qualitative comparison for the yearly average data of DNI and DHI obtained from Global Solar Atlas (A) vs the model predictions (B) using the cloud-cover proposed model. For a quantitative comparison, Table 2 shows the values obtained for cloud-cover parameters in estimating DNI and DHI and the NRMSE between the model and the validation data. The raw data used to generate the maps of Figs. 5 to 8 are available in an open dataset [38].

The model shows a better fitting for diffuse irradiation due to its low variability with longitude, but has a high dependency on the latitude factor (c_{DHI} absolute value is six times c_{DNI}, despite the values of DHI being lower). The value of a_{DHI} shows that there is a minimal diffuse light, scattered by the atmosphere even on sunny days. The change in the sign of c parameters means that the latitude effect works similarly to that of cloud-cover, probably based on the humidity of clouds (increasing or decreasing their scattering and absorption). The standard error of parameters also reflects a good fitting and high statistical relevance of the chosen independent variables.

Using the parameters in Table 2, the time-varying values of total radiation (GHI and TIR) can be used to obtain yearly averaged values and thus allow to validate the model against the data available in the Global Solar Atlas. In each timestep, the zenith angle of the Sun was used to calculate the maximum theoretical horizontal irradiation, to allow an estimation of GHI using equation 11.

As GHI values are also available in Global Solar Data, the results were compared (Fig. 6), obtaining an NRMSE of 10.2%. The error is lower than those obtained in DNI or DHI, meaning that the main differences come from the distribution between direct and diffuse light, and not from total irradiation.

Equation 13 was applied in both the measured and estimated values (Fig. 6) to estimate TIR values. Results were also compared, obtaining an NRMSE of 8.3%. Once again, this value is lower than the individual errors of DNI and DHI, showing that the model accuracy in total radiation is better than in diffuse fraction of light.

Once temperature and radiation maps are calculated, the kinetic model can be applied to calculate the disinfection potential for each region.

Table 2
Parameters for cloud impact calculation and NRMSE obtained for DNI and DHI.

DNI NRMSE 20.5%		DHI NRMSE 12.6%	
Cloud impact parameter	Value	Cloud impact parameter	Value
a_{DNI}	$0.726 \pm 1.5 \times 10^{-3}$	a_{DHI}	$0.182 \pm 3.6 \times 10^{-4}$
b_{DNI}	$-5.55 \times 10^{-3} \pm 2.6 \times 10^{-5}$	b_{DHI}	$9.26 \times 10^{-5} \pm 6.4 \times 10^{-6}$
c_{DNI}	$-1.08 \times 10^{-4} \pm 9.9 \times 10^{-6}$	c_{DHI}	$6.77 \times 10^{-4} \pm 2.4 \times 10^{-6}$
R^2	0.958	R^2	0.985

3.4. SODIS inactivation of E. coli

The guidelines for SODIS require an exposure time of 6 h to achieve "protected" drinking water; this could be practically translated as the need to achieve a 4-log inactivation of bacterial pathogens [2]. As the inactivation kinetics are usually considered a first-order reaction rate, the target of 4-log is theoretically independent of the initial concentration. The transient values of temperature and irradiation were used in the kinetic model at all the locations in the 0.5° grid, every 90 timesteps per day, from sunrise to sunset, covering a full year. Three different indicators were considered to evaluate the inactivation results at every location: i) the daily number of batches (where a batch is considered the process of achieving 4-log inactivation); ii) the daily minimum SODIS time (required for complete a batch); and iii) the SODIS potential, calculated as the ratio between the standard 6 h requirement and the calculated minimum SODIS time. Although the validation of the radiation calculations was done between 60° North and 45° South to allow comparison with Global Solar Atlas reports, this study was extended to cover the region between 67.5° North (Arctic polar circle) and 55.5 ° South (latitude of Cape Horn).

To calculate the daily total number of batches, inactivation is integrated over time until it reaches a 4-log inactivation, starting again from that instant until sunset is reached. Then, a monthly average of this value is calculated and stored. For the minimum SODIS time,

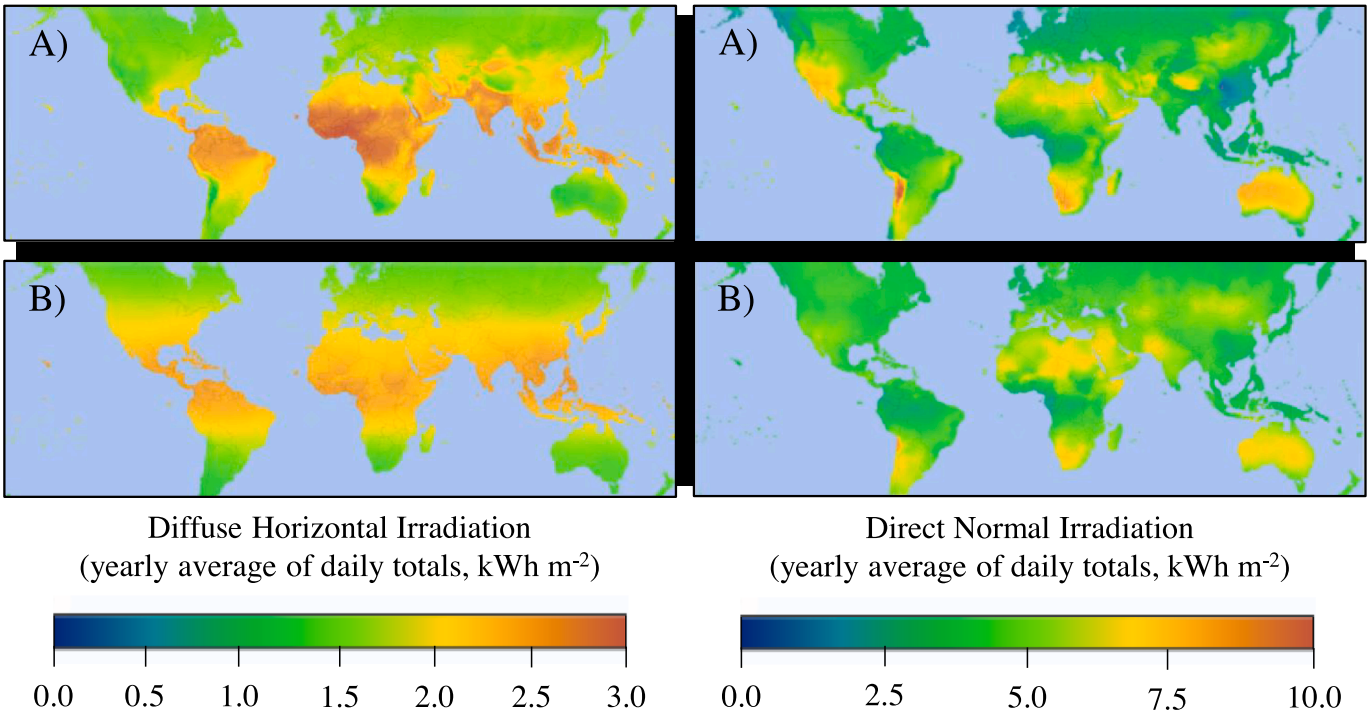

Fig. 5. World maps of yearly average daily totals. Left) Direct Normal Irradiation, Right) Diffuse Horizontal Irradiation. A) Global Solar Atlas. B) Model.

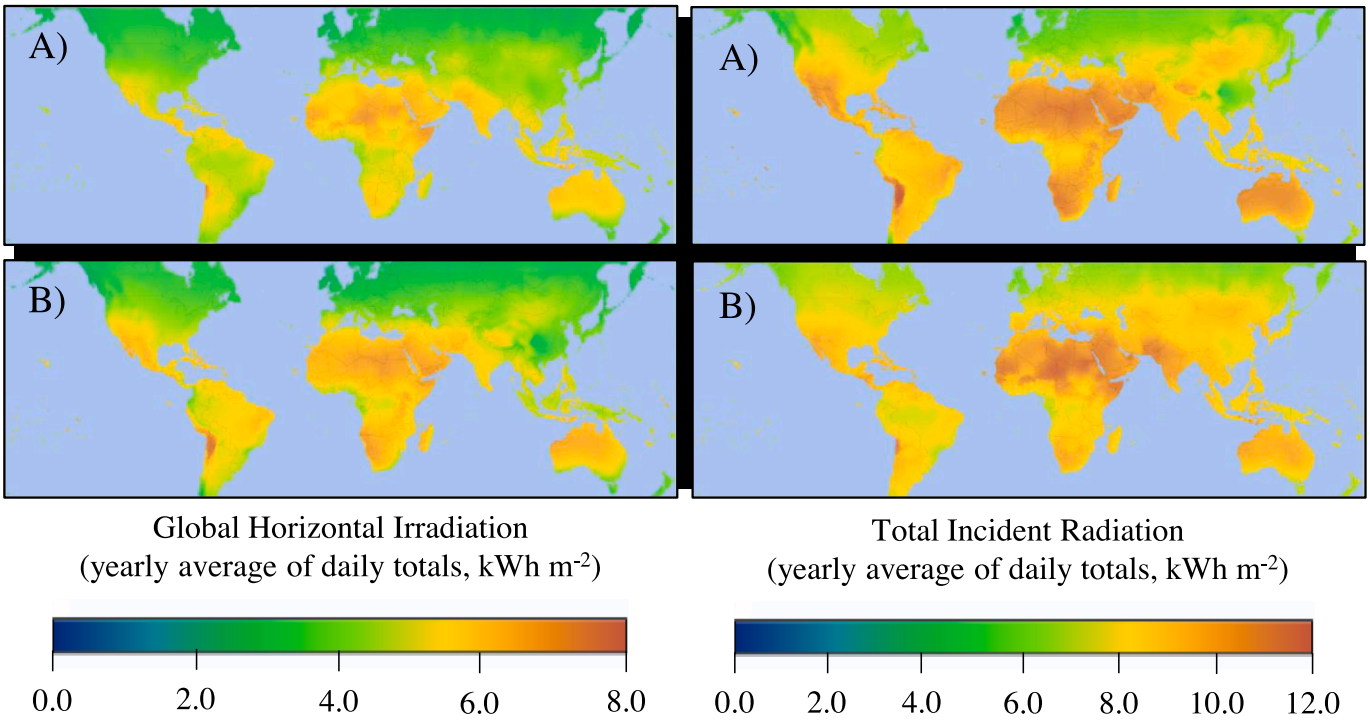

Fig. 6. World maps of yearly average daily totals. Left) Global Horizontal Irradiation. Right) Total Incident Radiation A) Global Solar Atlas. B) Model.

inactivation is evaluated starting from each timestep, choosing the shortest time to achieve the desired 4-log inactivation. SODIS potential is referred to this minimum SODIS time as a quantitative index of the suitability of the process.

Fig. 7 shows the summarised results of daily batches and SODIS minimum time. Data were calculated as monthly averages, but the figure shows the annual minimum, maximum and average values.

We note here that the contours of daily batches are limited to regions where at least one daily batch is achieved. If the annual minimum values of this indicator are observed, the coloured regions are those where SODIS can reach the desired inactivation all year long. These regions are located between 30 ° North and 30° South, except for certain specific points limited by low temperatures or high cloud-cover. The annual maximum shows that at any location between 80° North and 80° South there is at least one month of enough irradiation and temperature to achieve a single batch.

The annual maximum values of SODIS time show a narrow distribution around 6 h at most of the regions where a batch is achieved. This can be considered as a secure time for the SODIS process. Conversely, the annual average and minimum values show that the required time is significantly lower in several regions, meaning that several batches can be treated, or that the time window to carry out the process is wider.

Fig. 8 shows the yearly average value of SODIS potential worldwide, as a clear reference to the best locations to use the technology during the entire year. Figure S1 in the supplementary information shows the monthly averaged values throughout the year used to formulate this map, allowing the seasonal estimation of the required time and the potential impact of the technology in a region. According to the estimation process of the SODIS potential, regions with a SODIS potential less than 1 should apply a longer exposure than the standard six-hour time to guarantee the required microbial target inactivation.

While latitude has the main impact on the SODIS potential with an expected global trend where the potential decays as latitude grows, the map also shows the relevance of cloud coverage and temperature. Equatorial regions, with high cloud-cover most of the year, offer lower values than tropics, where low cloud-cover and high temperature are present at the same time. Regions with similar cloud-cover, but colder temperatures, lead to a low potential. In these cases, it is strongly suggested that SODIS is applied with caution.

3.5. Model limitations and broader applicability of the model

The proposed model is intended as a tool for preliminary evaluation of the potential in a region to use solar water disinfection, based on historical climatic and meteorological data, and not as an accurate model to predict the exact required exposure time, which obviously will depend on the weather conditions of the actual day of the treatment. Moreover, the reported kinetic model predicts the effect of radiation and temperature in wild type *E. coli* bacteria under relatively ideal natural water conditions. Therefore, the reported SODIS potential cannot be automatically extrapolated to other microorganisms, water composition and optically active container materials. However, the developed modular procedure can be easily adapted to any other specific scenario. Chemical matrix composition effects, such as iron salts, organic matter, low ionic strength, etc., can be included in the kinetic model. Alternative kinetic models based on fitting experimental data for inactivation of other microorganisms could be easily included. Similarly, optical effects of water turbidity and the container's absorption can also be easily included if required for a specific application [35]. For instance, in a region with a SODIS potential of 1.5, the potential could be significantly lower for water with high turbidity.

Finally, it is worth noting that dark repair of bacterial DNA is not considered impeding the model, as a treatment time higher than one solar day is evaluated as 0 batches in a day. On the other hand, the proposed methodology can be applied to any other solar photoactivated process different from solar water disinfection, such as photo-Fenton, semiconductor photocatalysis, solar/H_2O_2, solar/Cl_2, etc. The only aspect that should be considered in those cases is that, for systems with high optical density, absorbed radiation should be computed and used in the kinetic model instead of incident radiation.

4. Conclusions

In this work, we have developed a detailed methodology for

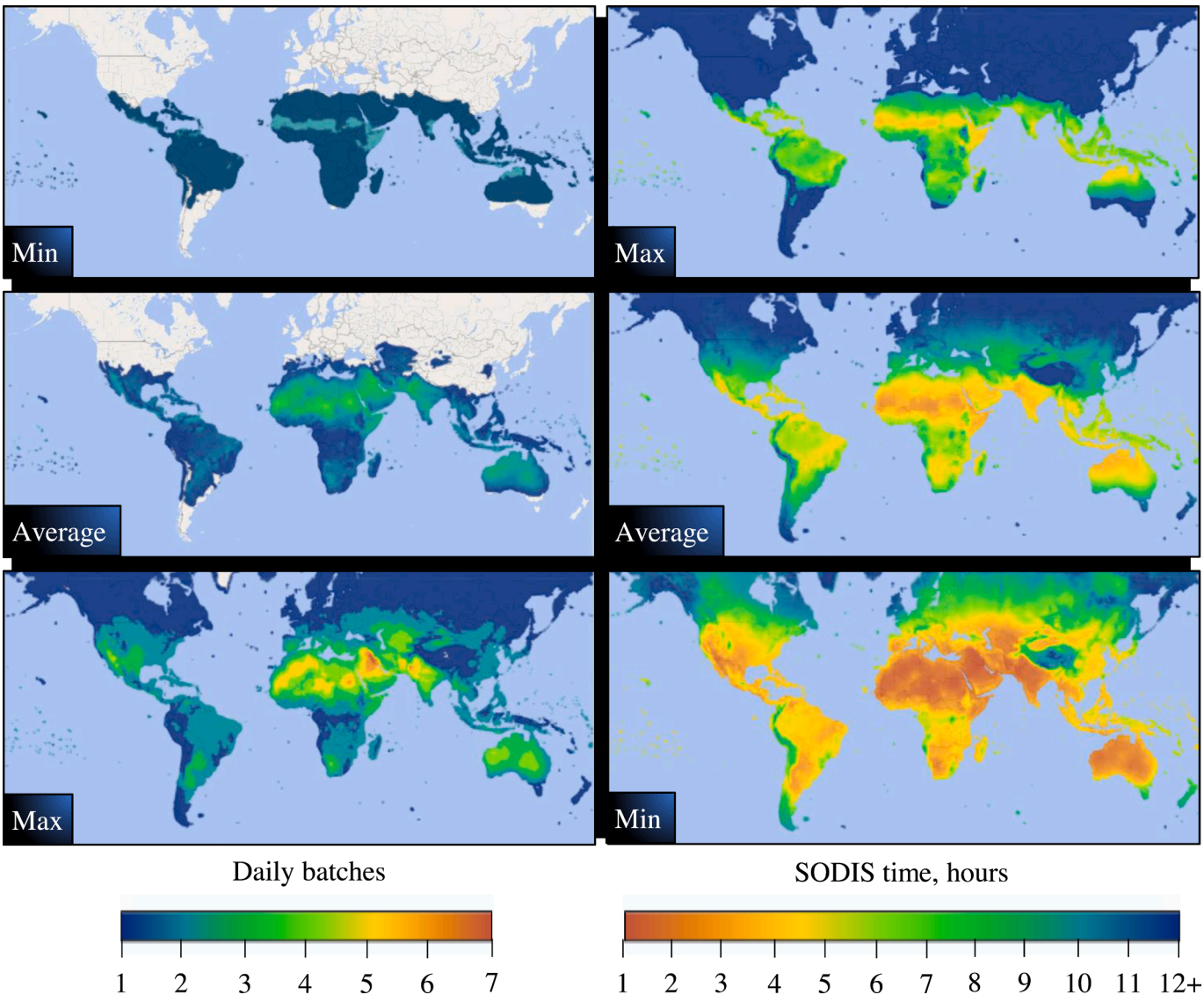

Fig. 7. World maps of predicted SODIS disinfection. Daily batches of 4-log disinfection (left), minimum SODIS time for 4-log disinfection (right).

estimating the success of solar disinfection. Using available open access libraries, we have succeeded in extracting time-varying radiation, temperature and cloud coverage data at any moment, anywhere in the world. A simple model describing the thermal/optical inactivation by solar light was used to fit *E. coli* inactivation laboratory data at different solar irradiation and temperature values. By introducing the instantaneous values of temperature, irradiance and cloud-cover into the developed model, SODIS-mediated bacterial inactivation can be easily estimated. Furthermore, this transient estimation was extended throughout the year, which provided a metric that computes the chances of a successful solar treatment intervention method, the SODIS potential.

The developed tool can significantly contribute to understanding the suitability and limitations of the SODIS process worldwide. The results show the relevance of a more in-depth study of the radiation and temperature conditions. The distribution is more complex than simple latitude bands, and time-varying values are required to evaluate the performance of solar water disinfection processes properly.

The developed SODIS potential maps present a global error in the predicted logarithmic inactivation below 8% regarding the solar calculations. However, the kinetic constants' prediction has an inherently higher uncertainty associated with the variable microorganisms and physicochemical factors in field applications. The proposed modelling approach is open to future improvements based on more rigorous descriptions of the inactivation mechanism that can be easily integrated into the whole predictive procedure. Additionally, the potential future availability of a SODIS database with results at different locations worldwide covering the whole range of the independent variables would further improve the model's predictive power.

This research opens the possibility for further expansion and a better estimation of the true SODIS capabilities. Based on this modular approach of independent calculation of solar irradiance, cloud-cover, temperature and microorganism inactivation components, the proposed tool can be easily customised to provide predictions on specific geocoordinates, date/time and alternative microbial indicators, such as viruses or protozoa. The model could also be adapted to describe other solar-based processes such as the photo-Fenton, persulfate activation or semiconductor photocatalysis and form a powerful tool in decision-making and water policy level around the sunny regions of the world.

Declaration of Competing Interest

The authors declare that they have no known competing financial interests or personal relationships that could have appeared to influence

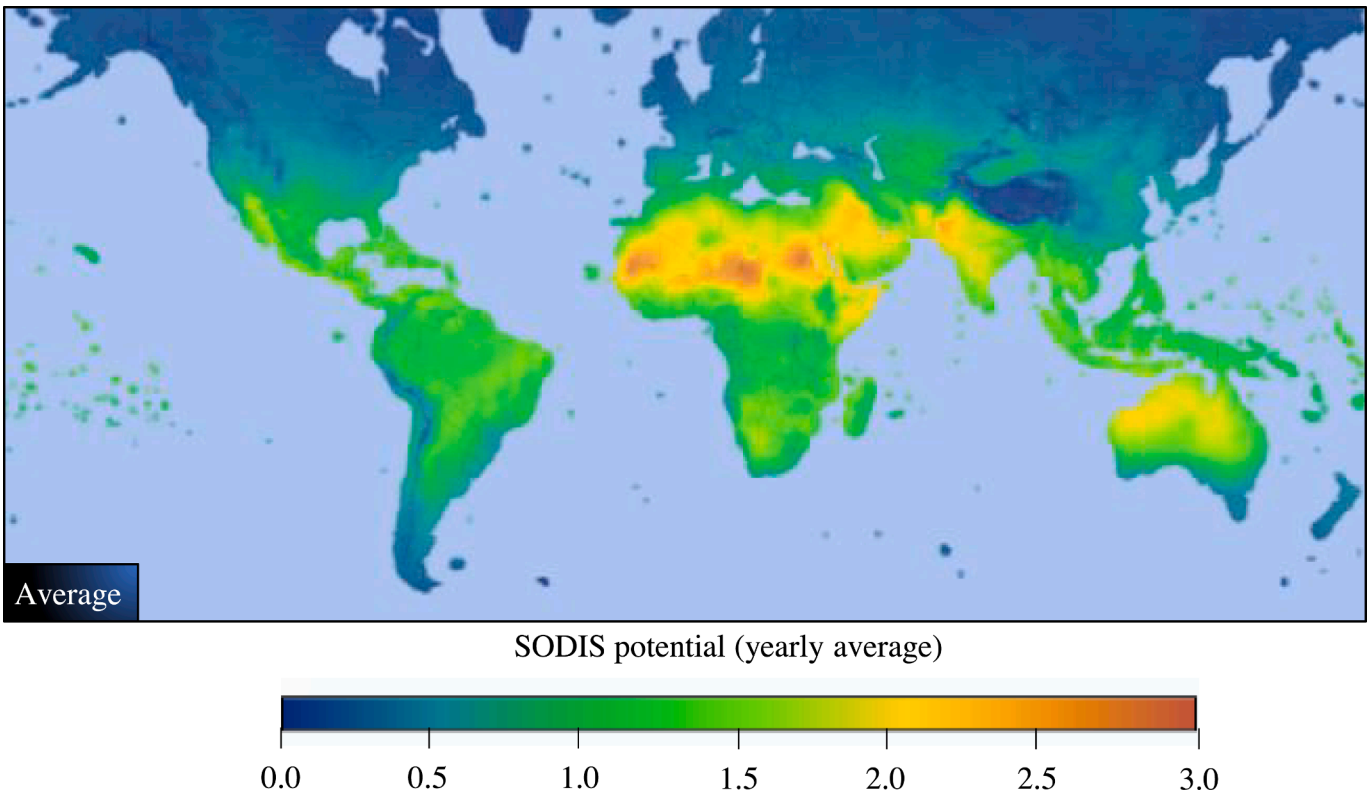

Fig. 8. World map of yearly average SODIS potential.

the work reported in this paper.

Acknowledgments

The authors gratefully acknowledge the financial support of Comunidad de Madrid and European Structural Funds [FOTOCAOS project, Y2018/EMT-5062] and the European Union's Horizon 2020 research and innovation programme in the frame of the PANIWATER project (GA 820718), funded under the Indo-EU International Water cooperation sponsored jointly by European Commission and Department of Science and Technology, India. Stefanos Giannakis acknowledges the Spanish Ministry of Science, Innovation and Universities (MICIU) for the Ramón y Cajal Fellowship (RYC2018-024033-I).

Appendix A. Supplementary data

Supplementary data to this article can be found online at https://doi.org/10.1016/j.cej.2021.129889.

References

[1] M. Sommer, B. Mariño, A. Solarte, Y. Salas, M.L. Dierolf, C. Valiente, C. Mora, D. Rechsteiner, R. Setter, P. Wirojanagud, W. Ajarmeh, H. Al-Hassan, A. Wegelin, SODIS-an emerging water treatment process, Water Supply Res. Technol. 46 (3) (1997) 127–137.

[2] K.G. McGuigan, R.M. Conroy, H.J. Mosler, M. du Preez, E. Ubomba-Jaswa, P. Fernandez-Ibañez, Solar water disinfection (SODIS): A review from bench-top to roof-top, J. Hazard. Mater. 235–236 (2012) 29–46, https://doi.org/10.1016/j.jhazmat.2012.07.053.

[3] R. Meierhofer, G. Landolt, Factors supporting the sustained use of solar water disinfection - Experiences from a global promotion and dissemination programme, Desalination 248 (1-3) (2009) 144–151, https://doi.org/10.1016/j.desal.2008.05.050.

[4] Á. García-Gil, C. Pablos, R.A. García-Muñoz, K.G. McGuigan, J. Marugán, Material selection and prediction of solar irradiance in plastic devices for application of solar water disinfection (SODIS) to inactivate viruses, bacteria and protozoa, Sci. Total Environ. 730 (2020), 139126, https://doi.org/10.1016/j.scitotenv.2020.139126.

[5] R.M. Tyrrell, S.M. Keyse, New trends in photobiology the interaction of UVA radiation with cultured cells, J. Photochem. Photobiol. B Biol. 4 (4) (1990) 349–361, https://doi.org/10.1016/1011-1344(90)85014-N.

[6] J. Marugán, R. van Grieken, C. Pablos, M.L. Satuf, A.E. Cassano, O.M. Alfano, Rigorous kinetic modelling with explicit radiation absorption effects of the photocatalytic inactivation of bacteria in water using suspended titanium dioxide, Appl. Catal. B Environ. 102 (3-4) (2011) 404–416, https://doi.org/10.1016/j.apcatb.2010.12.012.

[7] A.L. Santos, V. Oliveira, I. Baptista, I. Henriques, N.C.M. Gomes, A. Almeida, A. Correia, Â. Cunha, Wavelength dependence of biological damage induced by UV radiation on bacteria, Arch. Microbiol. 195 (1) (2013) 63–74, https://doi.org/10.1007/s00203-012-0847-5.

[8] P.M. Oates, P. Shanahan, M.F. Polz, Solar disinfection (SODIS): Simulation of solar radiation for global assessment and application for point-of-use water treatment in Haiti, Water Res. 37 (2003) 47–54, https://doi.org/10.1016/S0043-1354(02)00241-5.

[9] C. Mohácsi-Farkas, J. Farkas, L. Mészáros, O. Reichart, É. Andrássy, Thermal denaturation of bacterial cells examined by differential scanning calorimetry, J. Therm. Anal. Calorim. 57 (1999) 409–414, https://doi.org/10.1023/A:1010139204401.

[10] R.L. Annear, S.A. Wells, A comparison of five models for estimating clear-sky solar radiation, Water Resour. Res. 43 (2007), https://doi.org/10.1029/2006WR005055.

[11] C. Gautier, G. Diak, S. Masse, A simple physical model to estimate incident solar radiation at the surface from GOES satellite data, J. Appl. Meteorol. 19 (8) (1980) 1005–1012, https://doi.org/10.1175/1520-0450(1980)019<1005:ASPMTE>2.0.CO;2.

[12] ANSYS FLUENT Theory Guide, 15317 (2012) 724–746.

[13] V.H. Mantzari, D.H. Mantzaris, Solar radiation: Cloudiness forecasting using a soft computing approach, Artif. Intell. Res. 2 (2012), https://doi.org/10.5430/air.v2n1p69.

[14] P.M. Ferreira, A. Ruano, E.M. Crispim, A.E. Ruano, Prediction of the solar radiation evolution using computational intelligence techniques and cloudiness indices Intelligent Control of Air Conditioning Systems in Buildings, CISCE) View project Intelligent algorithms for classification of biosignals View p, Int. J. Innov. Comput. Inf. Control ICIC., 2007.

[15] S. Samoili, G. Farinelli, Ja. Moreno-SanSegundo, S. Giannakis, K. McGuigan, J. Marugán, C. Pulgarín, Dataset: SODIS performance on the inactivation of E. coli under different irradiance and temperature conditions. v.1.0.0, Zenodo. (2020). 10.5281/zenodo.4632759.

[16] K.G. McGuigan, T.M. Joyce, R.M. Conroy, J.B. Gillespie, M. Elmore-Meegan, Solar disinfection of drinking water contained in transparent plastic bottles: characterizing the bacterial inactivation process, J. Appl. Microbiol. 84 (1998) 1138–1148.

[17] Omatoyo K. Dalrymple, Elias Stefanakos, Maya A. Trotz, D. Yogi Goswami, A review of the mechanisms and modeling of photocatalytic disinfection, Appl. Catal. B Environ. 98 (1-2) (2010) 27–38.
[18] Leonard W. Hom, Kinetics of chlorine disinfection in an ecosystem, ASCE J. Sanit. Eng. Div. 98 (1) (1972) 183–194.
[19] L.S. Lasdon, R.L. Fox, M.W. Ratner, Nonlinear Optimization Using the Generalized Reduced Gradient Method. Revue française d'automatique, informatique, recherche opérationnelle, RAIRO - Oper. Res. - Rech. Opérationnelle. 8 (1974) 73–103. http://www.numdam.org/item?id=RO_1974__8_3_73_0 (accessed November 9, 2020).
[20] K.C. Atwood, A. Norman, On the Interpretation of Multi-Hit Survival Curves, Proc. Natl. Acad. Sci. 35 (1949) 696–709. 10.1073/pnas.35.12.696.
[21] M. Castro-Alférez, M.I. Polo-López, J. Marugán, P. Fernández-Ibáñez, Mechanistic modeling of UV and mild-heat synergistic effect on solar water disinfection, Chem. Eng. J. 316 (2017) 111–120, https://doi.org/10.1016/J.CEJ.2017.01.026.
[22] ESMAP, SOLARGIS, WB, IFC, Global Solar Atlas, Glob. Sol. Atlas. (2019) 1. https://globalsolaratlas.info/map (accessed September 21, 2020).
[23] B. World, World Bank Group - International Development, Poverty, & Sustainability, World Bank. (2017). https://www.worldbank.org/.
[24] I. Harris, T.J. Osborn, P. Jones, D. Lister, Version 4 of the CRU TS monthly high-resolution gridded multivariate climate dataset, Sci. Data. 7 (2020) 109, https://doi.org/10.1038/s41597-020-0453-3.
[25] Weather.com, National and Local Weather Radar, Daily Forecast, Hurricane and information from The Weather Channel, (2019). https://weather.com/.
[26] Hugo Beltrami, On the relationship between ground temperature histories and meteorological records: A report on the Pomquet station, Glob. Planet. Change 29 (3-4) (2001) 327–348, https://doi.org/10.1016/S0921-8181(01)00098-4.
[27] National Renewable Energy Laboratory, Solar Position Algorithm| NREL, (2020). http://www.nrel.gov/mide/solpos.spa.html.
[28] Ibrahim Reda, Afshin Andreas, Solar position algorithm for solar radiation applications, Sol. Energy. 76 (5) (2004) 577–589, https://doi.org/10.1016/j.solener.2003.12.003.
[29] Andrew T. Young, Air mass and refraction, Appl. Opt. 33 (6) (1994) 1108, https://doi.org/10.1364/AO.33.001108.
[30] F. Kasten, A.T. Young, Revised optical air mass tables and approximation formula, Appl. Opt. 28 (1989) 4735, https://doi.org/10.1364/ao.28.004735.
[31] R.K. Reed, On estimating insolation over the ocean, J. Phys. Oceanogr. 7 (1977) 482–485. 10.1175/1520-0485(1977)007<0482:oeioto>2.0.co;2.
[32] ZekaİŞen, Angström equation parameter estimation by unrestricted method, Sol. Energy 71 (2) (2001) 95–107, https://doi.org/10.1016/S0038-092X(01)00008-1.
[33] J. Huang, M.B. McElroy, Contributions of the hadley and ferrel circulations to the energetics of the atmosphere over the Past 32 Years, J. Clim. 27 (2014) 2656–2666, https://doi.org/10.1175/JCLI-D-13-00538.1.
[34] WHO, International Scheme to Evaluate Household Water Treatment Technologies Harmonized Testing Protocol: Technology Non-Specific Version 2.1, 2018. www.who.int/entity/household_water/scheme/HarmonizedTestProtocol.pdf?ua=1.
[35] J. Moreno-SanSegundo, J. Marugán, Solar Calculator for SODIS Potential, (2021). 10.5281/zenodo.4632779.
[36] M. Castro-Alférez, M.I. Polo-López, J. Marugán, P. Fernández-Ibáñez, Mechanistic model of the Escherichia coli inactivation by solar disinfection based on the photo-generation of internal ROS and the photo-inactivation of enzymes: CAT and SOD, Chem. Eng. J. 318 (2017) 214–223, https://doi.org/10.1016/J.CEJ.2016.06.093.
[37] C. Casado, J. Moreno-SanSegundo, I. De la Obra, B. Esteban García, J.A. Sánchez Pérez, J. Marugán, Mechanistic modelling of wastewater disinfection by the photo-Fenton process at circumneutral pH, Chem. Eng. J. 403 (2021), 126335, https://doi.org/10.1016/j.cej.2020.126335.
[38] J. Moreno-SanSegundo, S. Giannakis, S. Samoili, G. Farinelli, K.G.. McGuigan, C. Pulgarín, J. Marugán, Dataset of the article entitled "SODIS potential: a novel parameter to assess the suitability of solar water disinfection worldwide" (2021). 10.5281/zenodo.4633109.